Journal of Catalysis 263 (2009) 228–238

Contents lists available at ScienceDirect

Journal of Catalysis

www.elsevier.com/locate/jcat

On highly active partially oxidized platinum in carbon monoxide oxidation over supported platinum catalysts

E.M.C. Alayon [a], J. Singh [a], M. Nachtegaal [b], M. Harfouche [b], J.A. van Bokhoven [a,*]

[a] Institute for Chemical and Bioengineering, ETH Zurich, 8093 Zurich, Switzerland
[b] Paul Scherrer Institute, General Energy Research Department, Laboratory for Energy and Materials Cycles, 5232 Villigen PSI, Switzerland

ARTICLE INFO

Article history:
Received 24 November 2008
Revised 5 February 2009
Accepted 12 February 2009
Available online 17 March 2009

Keywords:
In situ XAS
Carbon monoxide oxidation
Supported platinum catalysts
Active phase

ABSTRACT

In situ X-ray absorption spectroscopy identified the role of oxidized platinum species in generating a high-activity state in the oxidation of carbon monoxide over Pt/Al_2O_3, Pt/TiO_2 and Pt/SiO_2. Two activity regimes were identified: low-activity at high carbon monoxide concentration and low temperature, and high activity at low carbon monoxide concentration and high temperature. The change between the two regimes occurred suddenly; there was ignition when going from low to high activity, and extinction from high to low activity. Ignition only occurred when the concentration of oxygen was higher than that of carbon monoxide. The catalyst was metallic and covered with carbon monoxide at low activity and partially oxidic at high activity. Carbon monoxide poisoned the catalyst at low activity. The partially oxidized platinum catalysts showed high activity. The partially oxidized catalyst had a lower oxygen coordination number and shorter Pt–O bond length as expected for bulk PtO_2, suggesting that a strongly defected platinum oxide was formed with a possibly square planar coordination. The catalyst structure showed a dynamic behavior and the amount of oxide depended on the concentration of reactants in the gas phase. Smaller particles of Pt/Al_2O_3 reached high activity at lower temperature than the larger particles. Pt/TiO_2 reached high activity at the lowest temperature while Pt/SiO_2 required the highest temperature. Parallel with the temperature of ignition, Pt/SiO_2 was the most oxidized while Pt/TiO_2 was the least oxidized.

1. Introduction

The catalytic properties of platinum remain one of the most fascinating subjects of study. While it belongs to the family of noble metals because of its rarity in the earth's crust and its resistance to corrosion, it has a different chemical behavior than the other noble metals copper, silver, and gold. Its extended d-orbitals enable chemisorption of adsorbates that subsequently react and desorb to complete the catalytic cycle. In spite of the wide importance platinum has gained in industry, and the extensive research performed on its catalytic behavior, the fundamental aspects of adsorption, reaction, and desorption that occur at its surface continue to be debated. Understanding what is happening at the catalyst surface and what the structure of the catalytically active phase is, are important for controlling the kinetics of the reaction in terms of activity, selectivity, and stability. Structural characterization is most relevant when performed under reaction conditions, which is generally at high pressure and temperature [1]. X-ray absorption spectroscopy (XAS) is an element-specific technique that enables structural analysis under catalytically relevant conditions [2,3]. The Pt L_3 whiteline, which is the first intense feature in the spectrum, is sensitive to the oxidation state of the catalyst as it reflects the empty d-density of states. The Pt L_3 X-ray absorption near-edge structure (XANES) is also sensitive to the local geometry and to the presence of adsorbates on the surface of the nanoparticles and the shape of the whiteline reveals the mode of adsorption [4–6]. The extended X-ray absorption fine structure (EXAFS) function is dependent on the local structure of the absorbing platinum atom. It provides coordination number, inter-atomic distance, and Debye–Waller factor [2].

The catalytic oxidation of carbon monoxide is the key reaction during the preferential oxidation of carbon monoxide in a hydrogen feed gas mixture in fuel cells, where it is crucial to decrease the carbon monoxide concentration below 50 ppmv [7]. It is also one of the reactions occurring in a three-way catalytic converter, where the pollutant gases are transformed into less harmful ones. Despite the seeming simplicity of carbon monoxide oxidation, the structure of the catalyst and the mechanism at high activity are still debated. Structural transformation of the platinum catalyst during carbon monoxide oxidation, both on single crystals and supported particles, has been reported. On a single crystal of

* Corresponding author.
E-mail address: j.a.vanbokhoven@chem.ethz.ch (J.A. van Bokhoven).

0021-9517/$ – see front matter
doi:10.1016/j.jcat.2009.02.010

Pt(100) [8,9], a transformation occurs from a hexagonal phase to a (1×1) phase with islands of $c(2 \times 2)$ when going from a low to a high carbon monoxide surface concentration. This surface phase transition [8] has been identified to be the driving force for the kinetic oscillations in catalytic carbon monoxide oxidation because the adsorption properties of the surface switch with the transition. The experiments were carried out on clean single crystals under ultra-high vacuum in a system equipped with LEED, AES, and work function measurement facilities. A possible formation of an oxide was linked to the presence of surface impurities, thus the surface of the catalyst was repeatedly cleaned to suppress oxide formation. Later experiments performed with scanning tunneling microscopy [10] and surface X-ray diffraction [11] on a single crystal of Pt(110) surface near atmospheric pressure showed a roughening of the surface coinciding with a sudden increase in catalytic activity for carbon monoxide oxidation. This switching of surfaces was attributed to a change in the surface composition. When the carbon monoxide concentration dropped below a particular value, the surface oxidized. This oxidized surface showed higher catalytic activity than the metallic surface [10,11]. To mimic industrial supported catalysts, nanometer-sized metal particles of platinum were deposited on silica, titania and alumina in ordered arrays by electron beam lithography. Carbon monoxide oxidation was performed at a few hundred Torr in various carbon monoxide and oxygen ratios and the total pressure brought to atmospheric pressure with helium. The reaction became sustainable above an ignition temperature, at which new carbon monoxide species, which were active for oxidation, were identified [12]. However, because the oxidic species has less affinity for carbon monoxide adsorption and the enhancement of conversion occurred at high temperature, metallic platinum was identified as the active surface for carbon monoxide oxidation [13,14]. Oxidation was also associated with catalyst deactivation during oxidation rate oscillations. These oscillations corresponded with periodic oxidation and reduction of the silica-supported platinum catalyst [15]. From previous results the low surface concentration of carbon monoxide at high temperature enabled oxygen to react with the platinum surface, which switched the reaction from being limited by desorption of the carbon monoxide to a regime with a different rate limiting step. The result was a higher rate of reaction and a partially oxidized catalyst. The enhanced conversion of carbon monoxide depleted the gas phase carbon monoxide concentration further, which decreased the surface concentration of carbon monoxide. This increased the extent of surface oxidation and caused an autocatalytic ignition of the reaction [16].

The size of supported platinum particles strongly affects their catalytic performance [13,17,18]. Moreover, the type of support and the interface between particles and support influence the catalytic turnover [19–25]. Thus, the important factors controlling catalytic activity over platinum are particle size, support, and the active phase. It is our goal to determine the structure of the active catalyst under reaction conditions, and to determine the effect of particle size and that of the support. We compare the behavior of nano-sized platinum on Al_2O_3, TiO_2 and SiO_2 during the catalytic reaction and the influence of particle size in Pt/Al_2O_3 and determine their structure under catalytic conditions using in situ Pt L_3 XAS.

2. Experimental

2.1. Catalyst preparation and characterization

2 wt% Pt/Al_2O_3 was prepared by incipient-wetness impregnation. A solution of 0.197 g $Pt(NH_3)_4(NO_3)_2$ in 2.55 mL water was mixed with 5 g of Al_2O_3, which was dried overnight at 120 °C. The mixture was shaken for 30 min and dried at room temperature for 4 h. The precursor was calcined in a flow of air at 0.6 bar in two stages: at 200 °C for 4 h and then at 400 °C for 4 h. The catalyst was reduced in a flow of hydrogen at 450 °C for 2 h and then cooled in a flow of helium. Two sets of this catalyst were synthesized. 3 wt% Pt/TiO_2 was also prepared by incipient-wetness impregnation. A solution of 0.3 g of H_2PtCl_6 in 70 mL water, with the pH adjusted to 4–5 using NaOH, was added to 4.0 g of TiO_2. The solution was stirred for 2 h at 70 °C. The obtained paste was filtered and washed with 1 L of warm water (70 °C) and dried under vacuum. The catalyst was calcined in a flow of air: heated at 5 °C/min to 120 °C, remained at this temperature for 4 h, heated again at 5 °C/min to 400 °C, remained at this temperature for another 4 h, and cooled to room temperature in a flow of air. The catalyst was reduced in a flow of 50 mL/min hydrogen for 2 h at 200 °C and cooled down to room temperature in 10 mL/min of flowing helium. Another 2 wt% Pt/SiO_2 catalyst was synthesized by incipient-wetness impregnation. 40 mL water was added to 0.197 g of $Pt(NH_3)_4(NO_3)_2$. NaOH was added to adjust the pH to 10. The solution was mixed with 5 g of dried SiO_2 and stirred for 2.5 h, was filtered, washed with 1 L of warm water (70 °C), and dried at 100 °C for 5 h. The calcination was done in a similar way as for Pt/TiO_2 described above. The catalyst was reduced in 50 mL/min of flowing hydrogen for 2 h at 250 °C and cooled to room temperature in hydrogen flow.

The size and shape of the platinum nanoparticles were observed by transmission electron microscopy (TEM) with a Tecani F30 microscope operating at 300 kV. A detector attached to the Tecani microscope using energy-dispersive X-ray spectroscopy (EDX) confirmed the tiny bright spots as the platinum particles. These particles were measured, counted, and translated into a particle size frequency distribution.

2.2. Kinetics and XAS measurement

Each of the catalysts was sieved to 63–125 μm, before loading in a plug flow (tubular packed bed) reactor, which was 1.6 mm in internal diameter, and which could accommodate 18 to 21 mg of the supported platinum catalysts depending on their density. The reactor also functioned as a transmission and/or fluorescence cell for X-ray absorption spectroscopy [26]. In addition, 2 wt% Pt/Al_2O_3 catalyst was loaded in a thin bed reactor [27], which accommodated 150 mg of the catalyst. This cell also functioned as

Table 1
Summary of catalytic properties of supported platinum catalysts in the oxidation of carbon monoxide.

Catalyst	Particle size (nm)	wt% platinum	Amount of catalyst (mg)	Platinum loading (mg)	Ignition temperature (°C)	Extinction temperature (°C)	Hysteresis (°C)
s-Pt/Al_2O_3	0.9	2	18.4	0.4	204	195	9
b-Pt/Al_2O_3	2.0	2	18.0	0.4	226	191	35
b-Pt/Al_2O_3[a]	2.0	2	150.0	3.0	169	115	40
Pt/TiO_2	1.3	3	21.2	0.6	188	145	43
Pt/SiO_2	1.9	2	18.0	0.4	299	281	18

[a] Measured in thin bed reactor.

Table 2
Gas treatment and reaction conditions.

Step	Gas	Flow (mL/min)	Temperature ramp (°C/min)	Temperature (°C)
Reduction sequence				
1	He	30.0	–	35
2	10% H_2/He	30.0	5	–
3	10% H_2/He	30.0	–	200
4	He	30.0	–	200
5	He	30.0	5	–
6	He	30.0	–	35
Heating to maximum CO conversion				
7	10% O_2/He	10.0	2	ramp
	CO	1.0		
	He	19.0		
Increasing CO flow				
8	10% O_2/He	10.0	0	–
	CO	1.25		
	He	18.75		
Cooling to room temperature				
9	10% O_2/He	10.0	2	ramp
	CO	1.0		
	He	19.0		

a transmission cell for XAS. Table 1 summarizes the catalyst loadings. All gases used were from Messer and were of high purity (>99.995 vol%). Mass flow controllers were calibrated with a digital flow meter. A mass spectrometer (GSD 300 O2, OmniStar, from Pfeiffer Vacuum) was attached at the end of the reactor for product gas analysis. Before a reaction, the catalyst was reduced in a sequence shown in Table 2. The total gas flowrate was always 30 mL/min corresponding to a space velocity of 0.06 s through the catalyst bed or a weight hourly space velocity (WHSV) of 15 to 26 $g_{gas}\,h^{-1}\,g_{cat}{}^{-1}$ depending on the gas mixture and catalyst loading in the plug flow reactor. After the pretreatment, a reactant gas mixture consisting of 10 mL/min of 10% oxygen in helium, 1 mL/min of carbon monoxide, and 19 mL/min of helium was fed to the reactor. This corresponds to a three percent carbon monoxide feed and an oxygen/carbon monoxide ratio of one. Temperature was ramped up using 2 °C/min until a 100% conversion in carbon monoxide was observed from the mass spectrometer traces of carbon monoxide, oxygen, and carbon dioxide. At two to five degrees higher than the temperature of maximum conversion, the carbon monoxide flow was increased to 1.25 mL/min, yielding a four percent carbon monoxide in the feed, while maintaining the total flowrate at 30 mL/min. This resulted in a conversion in carbon monoxide of less than 100%. Flowrates were always returned to their initial values before the temperature was ramped down at 2 °C/min to room temperature.

2.3. In situ X-ray absorption spectroscopy

XAS measurements were performed at the X10DA (superXAS) beamline at the Swiss Light Source, Villigen, Switzerland. Energy scans were performed with a Si-111 double crystal monochromator. Beam size was approximately 100 by 115 μm. Spectra were collected either in fluorescence or transmission geometry depending on the support. The first ionization chamber was filled with helium to detect the initial intensity; the second ionization chamber with a mixture of helium and nitrogen to detect the transmitted X-rays. A platinum foil was placed between the second ion chamber and a silicon diode for internal energy calibration. In fluorescence mode, a 13-channel germanium detector was used. During ramping up and down the temperature, XANES spectra were recorded from 11.545 to 11.600 keV. One XANES scan took four minutes, which corresponds to an eight degree span from start to finish using a ramp of two degrees per minute. Under stable temperature and flow conditions, EXAFS scans were recorded from 11.350 to 12.200 keV. It took about 30 min to complete one EXAFS scan. Multiple scans were averaged to improve the signal to noise ratio.

2.4. Data treatment

The traces for carbon monoxide, oxygen, and carbon dioxide, recorded by the mass spectrometer in terms of current, were divided by the helium signal for normalization. They were further processed to conversion curves against time or temperature. Conversion in carbon monoxide, (X_{CO}), was defined as

$$X_{CO} = \frac{\Phi_{v,CO,in} - \Phi_{v,CO,out}}{\Phi_{v,CO,in}},$$

where $\Phi_{v,CO,in}$ and $\Phi_{v,CO,out}$ were the flowrates of carbon monoxide at the inlet and outlet of the reactor respectively. The inlet flowrate was controlled by the mass flow controller. The outlet flowrate was derived from a calibration line assuming that the normalized signal at maximum conversion corresponded to 100% conversion, and that the normalized signal in the absence of conversion was the flowrate set at the inlet.

Data reduction for the XAS spectra was done using standard procedures [2,3]. It involved subtraction of the pre-edge background, edge energy determination, subtraction of the background signal from the spectra, and normalization of the edge jump to one. The data were processed using XDAP [28]. Previously generated reference files [29] were used to fit the EXAFS data. These were generated from the known unit cell parameters of platinum metal and platinum oxide using Atoms [30], calculated using the FEFF8 code [31] and fitted to actual XAS measured data of platinum foil and platinum oxide. Multiple shell fitting was performed in R-space ($1.5 < R < 3.5$) after Fourier transformation ($2.5 < k < 12$), and using a k-weighting of three for platinum–platinum scatterer pairs and two for the spectra that contained a mixture of platinum–oxygen and platinum–platinum pairs.

3. Results

3.1. Particle size

Fig. 1 shows TEM micrographs of the supported platinum catalysts. The little bright dots are the platinum particles and the larger light gray areas are the metal oxide supports. The platinum particles were well dispersed over all supports except silica. The small platinum on alumina particles (from here on referred to as s-Pt/Al_2O_3) were mainly 0.9 nm; the bigger platinum on alumina (b-Pt/Al_2O_3) particles 2.0 nm; the platinum on titania particles 1.3 nm, and the platinum on silica particles 1.9 nm. The particles on the latter support showed a significant fraction of larger particles.

3.2. Kinetic data

Table 1 summarizes the results of the kinetic measurements. Fig. 2 shows the normalized intensity signals from the mass spectrometer traces of carbon monoxide, oxygen, and carbon dioxide coming out of the reactor during carbon monoxide oxidation over s-Pt/Al_2O_3, and the temperature of the reactor. Fig. 3 displays the corresponding carbon monoxide conversion curve as function of temperature. The points marked with letters A to E in Fig. 2 correspond to those in Fig. 3. Starting at room temperature, the conversion of carbon monoxide increased exponentially with temperature. At 204 °C (B), a sudden jump in carbon monoxide conversion was observed and the catalyst reached a high activity state, at which the conversion in carbon monoxide was about

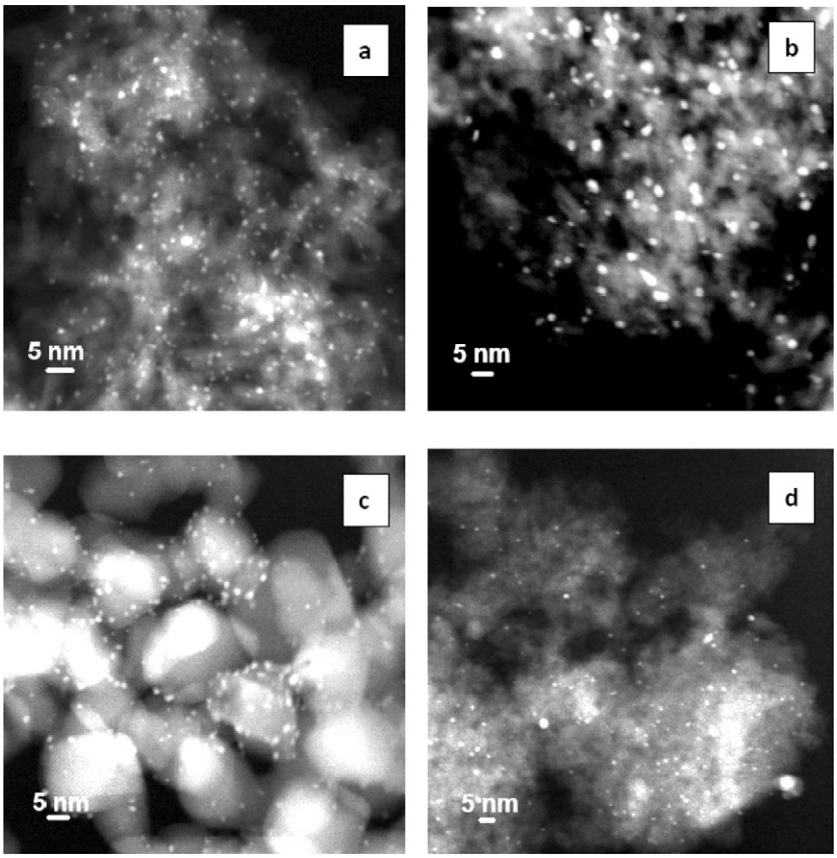

Fig. 1. TEM images of the supported platinum catalysts: (a) s-Pt/Al_2O_3, (b) b-Pt/Al_2O_3, (c) Pt/TiO_2, and (d) Pt/SiO_2.

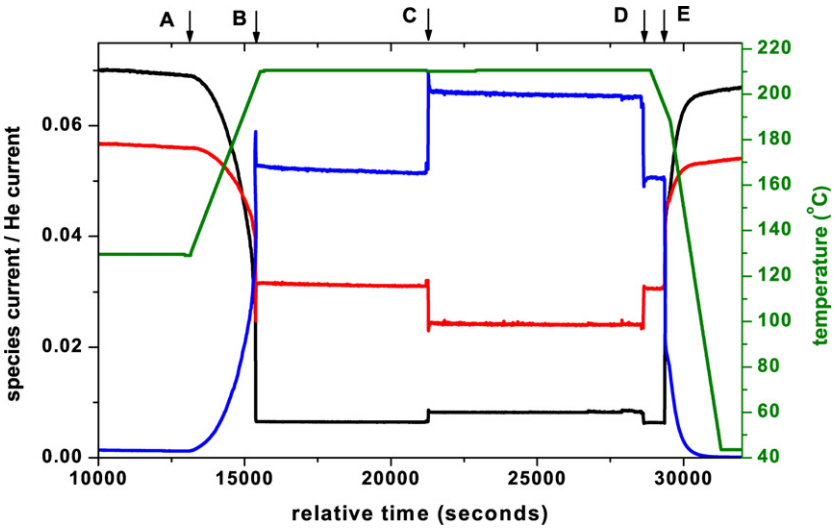

Fig. 2. Mass spectrometer traces of carbon monoxide (black), oxygen (red), and carbon dioxide (blue) normalized to the helium signal and the temperature profile (green) during carbon monoxide oxidation over s-Pt/Al_2O_3. (For interpretation of the references to color in this figure legend, the reader is referred to the web version of this article.)

54 mL/min/g_{cat} or 1.3×10^{21} molecules^{-1} min^{-1} g_{cat}. We call this jump ignition. At 21,200 s (C), the carbon monoxide flow was increased to 1.25 mL/min and the flow of helium was decreased to maintain the total flow at 30 mL/min. The resulting conversion was about 97%. At 28,800 s (D), the carbon monoxide and helium flows were returned to 1 and 18 mL/min respectively and the conversion returned to 100%. Upon decreasing temperature, a sudden jump to 42% conversion was observed at 195 °C (E). We call this reverse jump extinction and the catalyst returned to the low activity state. Hysteresis of 9 °C between the two activity regimes was observed. Ignition curves for carbon monoxide oxidation over a polycrystalline platinum wire were previously reported [32], but emphasis was more on the evolution of catalyst temperature with time. More recently, ignition and extinction during carbon monoxide oxidation over platinum were also identified [33], however these terms were used to identify the temperature at which 50% of carbon monoxide converted. This 50% conversion point is referred to as light-off temperature in literature. Carbon monoxide conversion curves with temperature, including a similar oxygen/carbon monoxide ratio were presented earlier [18] but only light-off conditions were iden-

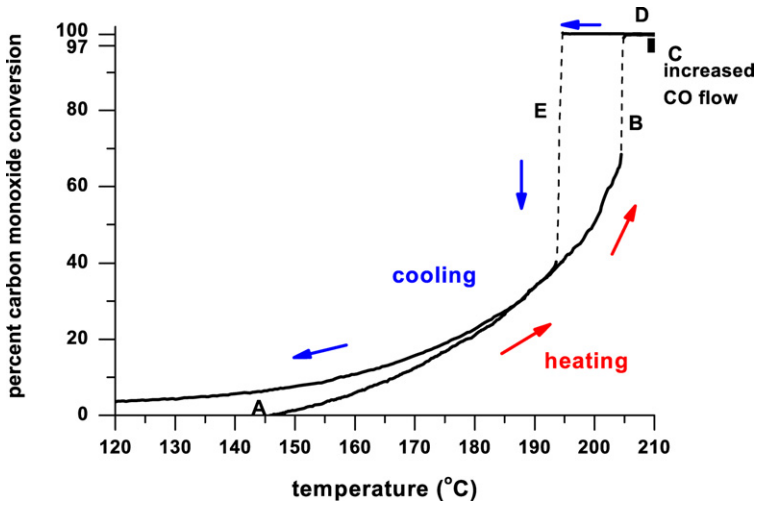

Fig. 3. Conversion plot of carbon monoxide with temperature over s-Pt/Al_2O_3.

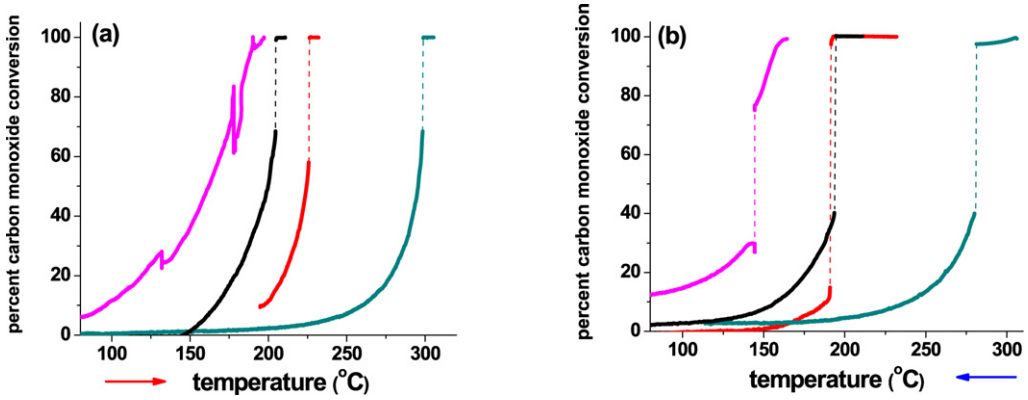

Fig. 4. Comparison of the heating (a) and cooling (b) curves for the different supported platinum catalysts: Pt/TiO_2 (pink), s-Pt/Al_2O_3 (black), b-Pt/Al_2O_3 (red), and Pt/SiO_2 (green). (For interpretation of the references to color in this figure legend, the reader is referred to the web version of this article.)

tified and not jumps in conversion. Ignition and extinction were indicated in the carbon monoxide conversion plots [34] where the relationships among the kinetic parameters under conditions of catalyst surface ignition during selective carbon monoxide oxidation on Pt/Ru/ceramic support were investigated.

For all catalysts reported in this manuscript, the trend is similar to that observed for the s-Pt/Al_2O_3 particles, however with distinctly different ignition and extinction temperatures. Fig. 4 shows the conversion plot against temperature during heating and cooling over the b-Pt/Al_2O_3, Pt/TiO_2, and Pt/SiO_2. During heating, the platinum catalyst supported on TiO_2 reached the high activity region at the lowest temperature. Ignition was at 188 °C, which was already near maximum conversion. The first two breaks in the conversion curve for Pt/TiO_2 correspond to the points where the temperature was held constant for about 1.5 h for taking EXAFS scans. Pt/TiO_2 switched to low conversion at 145 °C, which is the lowest extinction temperature of all catalysts measured here. Pt/SiO_2 required the highest temperature, 299 °C, to switch to the high activity region. Pt/SiO_2 jumped back to low activity also at the highest temperature, 281 °C. The b-Pt/Al_2O_3 and s-Pt/Al_2O_3 catalysts were intermediate between Pt/TiO_2 and Pt/SiO_2 in terms of activity and the temperatures required for ignition and extinction. The temperatures of ignition and extinction showed some variation upon varying the amount of catalyst, flow rate, and temperature ramps (data not shown). This indicates that ignition and extinction occur in an unstable reaction regime. Normal temperature behavior, without ignition and extinction, was observed when using a stoichiometric ratio of CO and O (data not shown).

The conversion of carbon monoxide was also determined with b-Pt/Al_2O_3 mounted in a thin bed reactor (data not shown). The switch from low to high activity and the inverse switch from high to low activity occurred at lower temperatures than when the same catalyst was mounted in the plug flow reactor (Table 1). After ignition, the conversion reached only about 70% probably because of unfavorable flow conditions. The total flowrate was double that of the plug flow by increased helium flow. The different observations cannot be attributed solely to the different flows and flow scheme in the two types of reactors, since the thin bed reactor contained much more catalyst than the plug flow reactor, 150 mg versus 18.0 mg.

3.3. XANES spectra

Fig. 5 shows the Pt L_3 XANES spectra of platinum in the metallic and in the Pt^{4+} oxidized state. In the metallic state, the whiteline showed a maximum absorption of 1.25, less compared to that in the oxidic state of 2.25. The metallic spectrum showed two bands at 11.580 and 11.596 keV immediately after the whiteline region. The oxidic spectrum showed a characteristic dip after the whiteline, and showed fine structure at 11.582 and 11.590 keV.

Figs. 6a and 6b compare the Pt L_3 XANES spectra measured while heating and cooling s-Pt/Al_2O_3 under the flow of oxygen/carbon monoxide with a ratio of one at various temperatures. The indicated temperatures refer to the beginning of each scan. The spectrum at 145 °C was taken in an atmosphere of helium after reduction and removal of hydrogen. The spectrum showed a

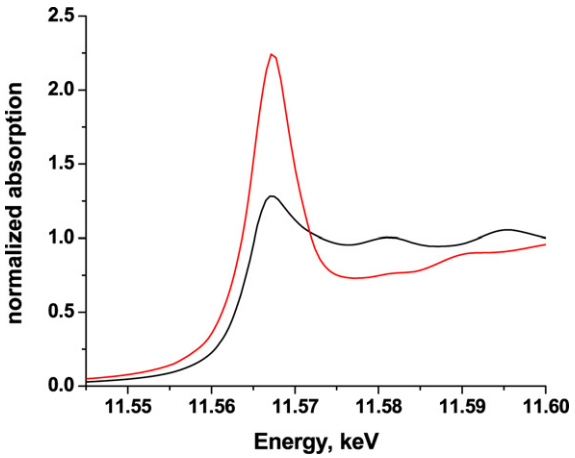

Fig. 5. Pt L_3 XANES of references: α-PtO_2 (red), and platinum foil (black). (For interpretation of the references to color in this figure legend, the reader is referred to the web version of this article.)

whiteline intensity similar to that of the platinum foil in Fig. 5. The bands at energies above the whiteline were subdued compared to that of the platinum foil spectrum but the characteristic feature of the wiggles was the same. This spectrum shows that the small platinum particles were in a reduced state after reduction and removal of hydrogen. The spectrum at 150 °C was obtained in a mixed carbon monoxide and oxygen atmosphere. Compared to the one recorded in helium, there was an increase in intensity and broadening of the whiteline to the high energy side, which is indicative of platinum with carbon monoxide adsorbed on the surface [6,16]. The features after the absorption edge overlapped those of the spectrum in helium, indicating the metallic character of the catalyst under these conditions. The spectrum measured at 174 °C shared the same features as the one at 150 °C but with a slightly decreased broadening of the whiteline indicating that part of the carbon monoxide was desorbed from the surface. The spectrum taken at 198 °C, which was at 46% conversion, started with a shape that resembled that of metallic platinum with carbon monoxide adsorbed on the surface, however, at 11.571 keV, it suddenly changed to that of an oxide. This corresponds to the tem-

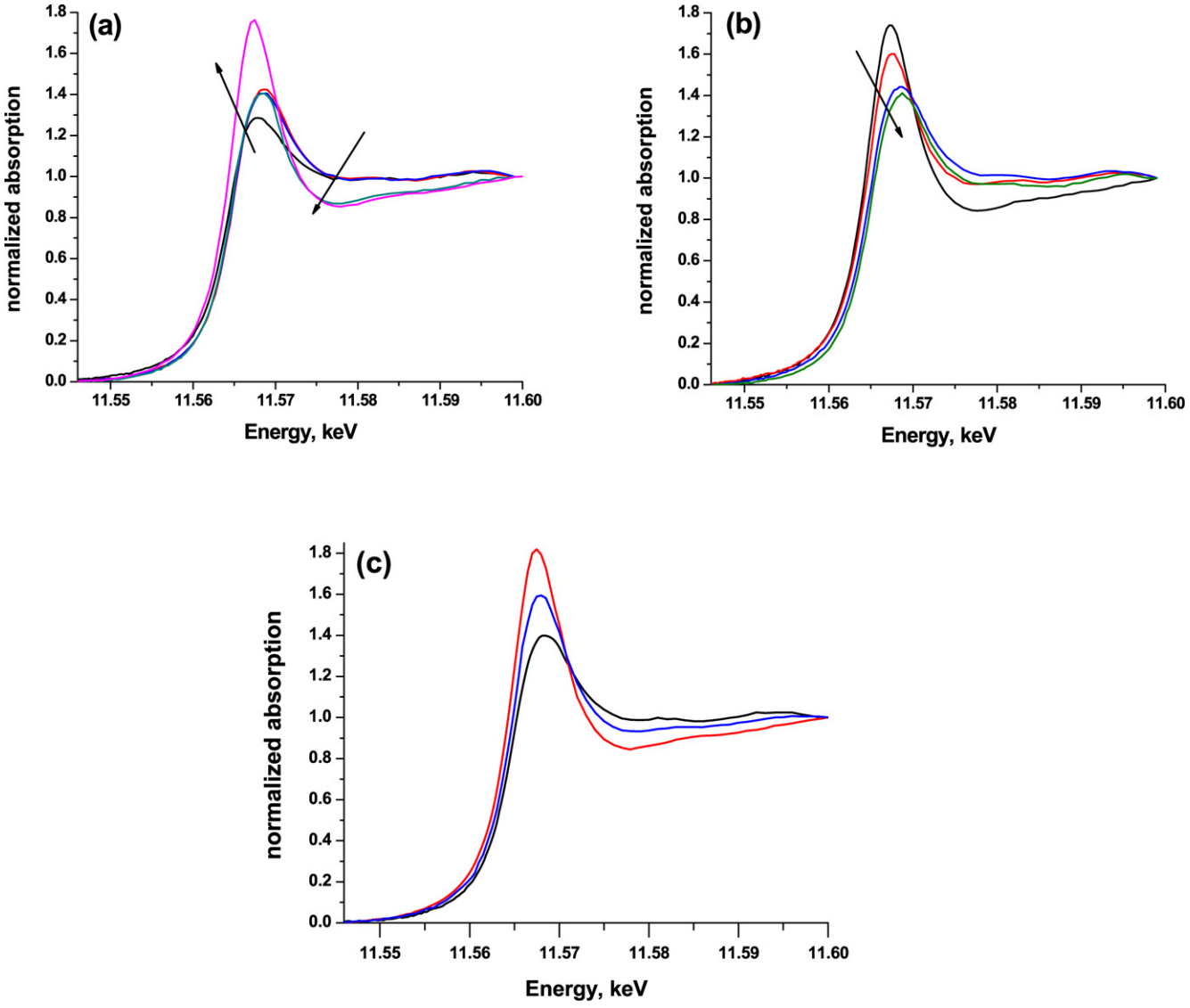

Fig. 6. Pt L_3 XANES spectra recorded during heating (a) at 145 °C in helium (black), 150 °C in oxygen and carbon monoxide (red), 174 °C (blue), 198 °C (green), and 211 °C (pink), during cooling (b) at 207 °C (black), 199 °C (red), 183 °C (blue), and 83 °C (green), and at the region of high activity (c) below ignition at 190 °C (black), above ignition at 211 °C and 100% conversion (red), and above ignition at 210 °C and 97% conversion (blue) of s-Pt/Al_2O_3; ignition occurred at 204 °C, extinction at 195 °C. (For interpretation of the references to color in this figure legend, the reader is referred to the web version of this article.)

perature of ignition of 204 °C, which correlates to point B in Figs. 1 and 2. The rapid change in rate of reaction is paralleled by fast structural changes of the platinum, as observed with time resolved XAS [16]. The spectrum taken at 211 °C, which is above ignition, had characteristic features of the spectrum of oxidized platinum in Fig. 5. The maximum intensity of the whiteline was 1.8, which is less than that of the Pt^{4+} spectrum, indicating that either the oxidation state is less than +4 or that there are still metallic platinum species left in the catalyst under these conditions. During cooling, the shape of the spectrum taken at 207 °C and above extinction showed an intense whiteline and the characteristic dip after the absorption edge. The scan taken at 199 °C with a conversion of 100% started with the intense whiteline feature of an oxide and at 11.573 keV shifted to the wiggles of the metallic spectrum after the edge, which again corresponds to the point of extinction at 195 °C, when the conversion jumped down to 41%, which is point E in Figs. 1 and 2. The other two scans recorded at lower temperatures 183 °C (26% conversion) and 83 °C (2% conversion) showed low whiteline intensity and small features above the edge. They also showed the broadened whiteline region characteristic of carbon monoxide adsorbed on the surface.

Fig. 6c shows the XANES spectrum taken above ignition at 97% conversion. The whiteline intensity is lower than that of the spectrum at above ignition at 100% conversion, yet higher than that at below ignition. The post-edge line is lower than the one at below ignition, with features similar to the post-edge dip and subtle curves of that at 100% conversion. The overall features of this spectrum show a shape similar to the oxidic spectrum with a reduced whiteline intensity, which suggests a reduced extent of oxidation.

In summary, the changes in the shapes of the spectra during cooling were opposite to those observed during heating. Above the temperature of ignition, the spectra showed elements of oxidized platinum, even after increasing the carbon monoxide concentration, such that no full conversion was reached. Below the ignition and extinction temperatures the spectra resembled those of carbon monoxide adsorbed platinum nanoparticles.

Fig. 7 shows the XANES spectra taken at increasing and decreasing temperature over b-Pt/Al_2O_3, Pt/TiO_2, and Pt/SiO_2. The same trends are observed. All spectra below ignition temperature showed the less intense and broadened whiteline of metallic platinum with carbon monoxide adsorbed on the surface, the amount of which decreases with temperature. Above ignition, the whiteline increased intensity similar to that of an oxidic species. The spectra were of metallic character at low activity and then switched to having oxidic features at high activity. The change to the oxidic features was a function of the temperature of ignition. The increase in the whiteline intensity was most pronounced for Pt/SiO_2, which ignited at the highest temperature, and the lowest increase was observed for Pt/TiO_2, which ignited at the lowest temperature. Upon decreasing the temperature, just above extinction, the conversion decreased for b-$PtAl_2O_3$ and Pt/TiO_2, which was paralleled by a decrease in intensity of the spectral whiteline and thus lower extent of oxidation.

3.4. EXAFS fitting results

Fig. 8 shows the averaged and k^3-weighted EXAFS function and corresponding Fourier transform of the EXAFS spectra taken at room temperature under a flow of helium for b-Pt/Al_2O_3 big particles after reduction and removal of hydrogen. The fits (dotted lines) of these functions provided coordination number (7.5), Debye–Waller factor (0.0040 $Å^2$), inter-atomic Pt–Pt distance (2.72 Å), and edge shift (1.7 eV) (Table 3).

The structural parameters for the fits of all the EXAFS spectra taken during the stages of the carbon monoxide oxidation runs are presented in Table 3. The spectrum taken at room temperature and in flowing helium for s-Pt/Al_2O_3 showed a first shell dominated by a Pt–Pt backscattering pair, with coordination number of 5.5. This correlates to metallic platinum particles with an average size of about 1 nm [35]. The Pt–Pt distance was 2.72 Å, smaller than the 2.76 Å of bulk platinum, indicating that the platinum cluster contracts when the particle size is very small [35–38]. The EXAFS spectrum taken at a slightly higher temperature in the presence of oxygen and carbon monoxide shows an increased Pt–Pt distance to 2.77 Å and equal coordination number within the margin of error. Bond length relaxation occurred after the adsorption of carbon monoxide as supported by the XANES similar to what occurs after adsorption of hydrogen [36,38,39]. Above ignition, an additional Pt–O scatterer with a Pt–O distance of 1.99 Å was observed that agrees well with the Pt–O distances of the platinum oxides, especially PtO and Pt_3O_4 [40]. These fitting parameters are also in agreement with the XANES spectra in Fig. 6 that showed characteristic oxidic features of platinum above ignition. The Pt–Pt coordination number decreased to 2.0 and the Pt–Pt distance decreased to 2.71 Å. This Pt–Pt contribution appeared to be a combination of Pt–Pt contributions from the remaining metal core and from the oxide and was thus difficult to fit separately.[1] This Pt–Pt bond length was shorter as expected for PtO_2. At increased carbon monoxide flow and 97% conversion, the fit still showed the Pt–Pt and Pt–O contributions with a slight increase in the Pt–Pt coordination to 3.0 and a slight decrease in the Pt–O coordination to 1.2 in agreement with features in the XANES (Fig. 6c). The EXAFS fit of the spectrum that was recorded at room temperature again was dominated by Pt–Pt scattering. The coordination number of 5.6 was similar to the starting value of 5.5 when it was in helium. The distance was 2.76 Å compared to 2.72 Å when measured in helium, which is again attributed to the presence of adsorbed carbon monoxide that slightly expands the cluster. The Debye–Waller factor showed higher values at higher temperature and returned to almost its original value when cooled down to room temperature.

The b-Pt/Al_2O_3 catalyst, measured in the plug flow reactor at 35 °C in flowing helium, had a Pt–Pt coordination number of 7.5. This translates to a size of about 2 nm. The Pt–Pt distance increased slightly from 2.74 to 2.75 Å after introducing oxygen and carbon monoxide at 125 °C. The increase in bond length is less pronounced for the big particles than for the small particles. Fits of spectra recorded above ignition showed the presence of a Pt–O scatterer and decreased Pt–Pt contribution. Cooling down to 42 °C, the spectrum returned to the Pt–Pt dominated fit. In comparison to the values at 35 °C and in helium, the coordination number is the same, 7.5, but the Pt–Pt distance stayed at 2.75 Å because of the influence of adsorbed carbon monoxide. For the same catalyst but mounted in a different reactor, the fit parameters above and below ignition were similar to that in the plug flow reactor, in agreement with the XANES spectra (not shown).

Fits of the Pt/TiO_2 EXAFS recorded at 35 °C in helium atmosphere showed a coordination number of 7.0, which corresponds to a size of about 1.3 nm. The 2.71 Å Pt–Pt distance was smaller than the bulk value of 2.76 Å, again indicative of contraction when decreasing particle size. Heating to 132 and 178 °C, in an oxygen and carbon monoxide environment, the Pt–Pt distance increased to 2.75 Å, the Debye–Waller factor increased, and the Pt–Pt coordination number remained 7.0. Above ignition, the Pt–Pt coordination number decreased to 6.1 along with a decrease in the Pt–Pt distance to 2.72 Å. A small Pt–O contribution with coordination number of 0.7 at 1.97 Å was observed. After cooling to room temperature, the Pt–Pt dominated spectrum returned: the coordi-

[1] Pt–Pt contribution could also be fitted with combined contributions from a short Pt–Pt and a long Pt–O–Pt bond.

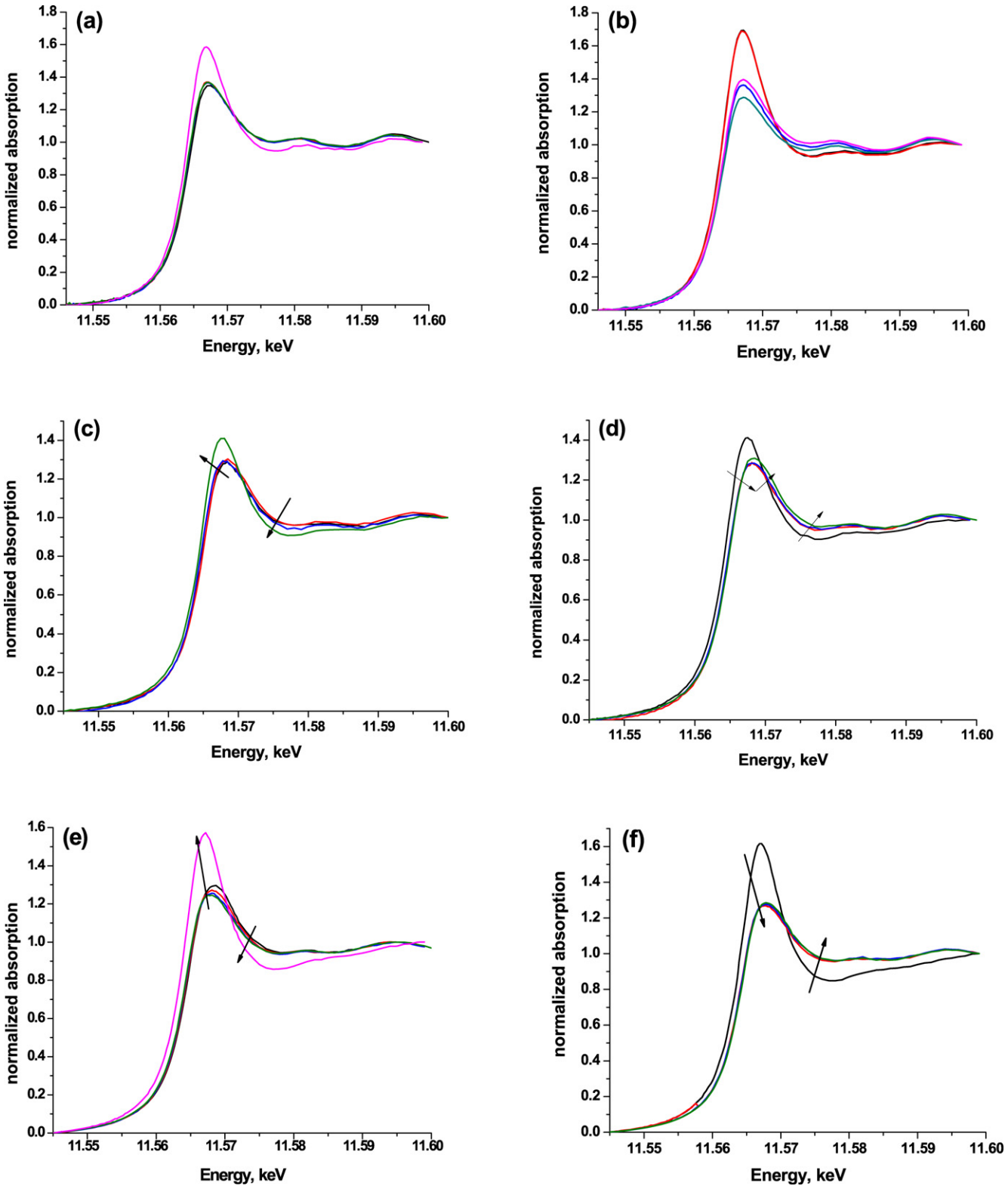

Fig. 7. Pt L_3 XANES spectra recorded during heating (a) at 125 °C (black), 194 °C (red), 210 °C (blue), 218 °C (green), and 231 °C (pink), and cooling (b) at 232 °C (black), 213 °C (red), 185 °C (blue), 156 °C (green), and 111 °C (pink) of b-Pt/Al_2O_3; ignition occurred at 226 °C, extinction occurred at 191 °C; Pt L_3 XANES spectra recorded during heating (c) at 68 °C (black), 134 °C (red), 180 °C (blue), and 190 °C (green), and cooling (d) at 177 °C (black), 145 °C (red), 114 °C (blue), and 36 °C (green) of Pt/TiO_2; ignition occurred at 188 °C, extinction occurred at 145 °C; Pt L_3 XANES spectra recorded during heating (e) at 40 °C (black), 140 °C (red), 240 °C (blue), 294 °C (green), and 306 °C (pink), and cooling (f) at 296 °C (black), 286 °C (red), 236 °C (blue), and 106 °C (green) of Pt/SiO_2; ignition occurred at 299 °C, extinction occurred at 281 °C. (For interpretation of the references to color in this figure legend, the reader is referred to the web version of this article.)

nation number became 6.9, which is similar to the values below ignition at various temperatures. The Pt–Pt distance also returned to 2.75 Å.

For Pt/SiO_2 at 35 °C in helium, coordination number was 7.6 and the Pt–Pt distance was 2.77 Å, which were quite similar to those of b-Pt/Al_2O_3 (2.0 nm) under the same conditions. Above

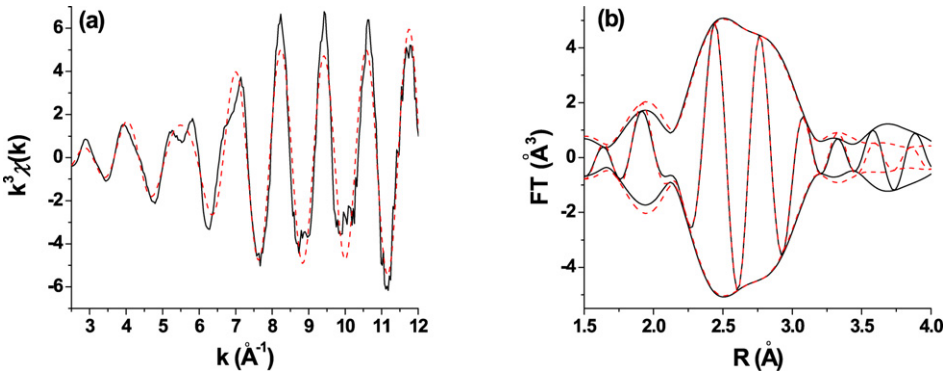

Fig. 8. (a) k^3-Weighted chi function and (b) corresponding Fourier transform (k^3-weighted, $2.5 < k < 12$ Å^{-1}) of b-Pt/Al_2O_3 experimental data (solid line) and fit (dashed line) in flowing helium at room temperature.

Table 3
EXAFS fitting results.

Conditions		Ab–Sc pair	N	DW (Å^2)	R (Å)	ΔE_0 (eV)	Goodness of fit
Temp. (°C)	Gas						
s-Pt/Al_2O_3 (0.9 nm)							
35	He	Pt–Pt	5.5	0.0040	2.72	1.7	5.0
129	O_2/CO	Pt–Pt	5.7	0.0047	2.77	0.5	14.9
211	O_2/CO	Pt–O	2.4	0.0025	1.99	3.2	104.3
		Pt–Pt[a]	2.0	0.0050	2.71	−1.4	
210	O_2/CO	Pt–O	1.2	0.0025	1.98	1.7	51.3
		Pt–Pt	3.0	0.0050	2.71	2.6	
38	O_2/CO	Pt–Pt	5.6	0.0038	2.76	1.9	11.2
b-Pt/Al_2O_3 (2.0 nm) in plug flow reactor							
35	He	Pt–Pt	7.5	0.0004	2.74	0.3	18.0
125	O_2/CO	Pt–Pt	7.8	0.0010	2.75	0.7	32.3
231	O_2/CO	Pt–O	1.3	0.0025	1.96	3.6	36.7
		Pt–Pt	6.7	0.0047	2.72	1.6	
232	O_2/CO	Pt–O	1.4	0.0025	1.97	3.9	33.5
		Pt–Pt	6.7	0.0047	2.72	1.9	
42	O_2/CO	Pt–Pt	7.5	0.0004	2.75	0.4	17.6
Pt/TiO_2							
35	He	Pt–Pt	7.0	0.0018	2.71	1.6	13.4
132	O_2/CO	Pt–Pt	7.0	0.0037	2.75	1.1	21.0
178	O_2/CO	Pt–Pt	7.0	0.0040	2.75	1.1	20.0
190	O_2/CO	Pt–O	0.7	0.0026	1.97	3.6	22.9
		Pt–Pt	6.1	0.0050	2.72	1.7	
36	O_2/CO	Pt–Pt	6.9	0.0018	2.75	1.8	26.8
Pt/SiO_2							
35	O_2/CO	Pt–Pt	7.6	0.0035	2.77	0.2	23.0
305	O_2/CO	Pt–O	3.1	0.0032	1.98	2.1	320.2
		Pt–Pt	2.3	0.0070	2.71	−1.8	
305	O_2/CO	Pt–O	3.7	0.0032	1.98	2.9	310.4
		Pt–Pt	2.0	0.0070	2.69	−1.1	

[a] Pt–Pt could also be fitted with two contributions of a short Pt–Pt at 2.60 Å and that of a long Pt–O–Pt at 3.15 Å.

ignition, the Pt–Pt coordination decreased to 2.3 and the Pt–Pt distance likewise decreased to 2.70. The Pt–O contribution appeared with a coordination number of 3.1 at 1.98 Å.

In summary, all catalysts showed an increase in Pt–Pt distance after switching from a flow of helium to one containing carbon monoxide. The platinum particles were in the metallic state at low conversion values as indicated by a Pt–Pt backscattering pair dominating the EXAFS functions and Fourier transforms. Above ignition, a Pt–O contribution appeared at a relatively short distance. A Pt–Pt contribution remained,[2] but with a shorter Pt–Pt distance than in a typical PtO_2; it resembled the Pt–Pt distance of metallic platinum. Thus the catalyst at above ignition consists of mixed oxide-metal phases, with the oxide most likely located at the surface. The higher the temperature of ignition, the larger was the fraction of oxidic platinum. Upon cooling to below the temperature of extinction, the structure of all catalysts returned to their original structure.

4. Discussion

4.1. Generating high activity

In the oxidation of carbon monoxide over supported platinum catalysts, two activity regimes are observed: a low-activity regime and a high-activity regime (Figs. 3 and 4). The low activity region occurs at low temperature and low carbon monoxide conversion. The high activity regime occurs at high temperature and high carbon monoxide conversion. Similar results had been reported during carbon monoxide oxidation on various forms of platinum-based catalysts: [10–12,33,41–44]. Some studies on carbon monoxide oxidation have been made by varying the oxygen and carbon monoxide partial pressures at fixed temperatures [10,11,44]. The changes in conversion in our study have been achieved by changing temperature at fixed inlet oxygen and carbon monoxide partial pressures.

The switch between high and low activity regimes is characterized by discontinuous changes in carbon monoxide conversion. The jump to high activity is called ignition, the reverse extinction. These switches are reversible but show hysteresis. The temperature of ignition is higher than the temperature of extinction. One reason may be the local heating of the platinum particles because of the exothermicity of the reaction. During the oxidation of methane over Pt/Al_2O_3, a comparison of the calculated and observed conversions had been made [45] and it appeared that platinum particles could be between 75 and 100 °C hotter than the average temperature detected by the thermocouple in the catalyst bed. A similar effect likely occurs in the carbon monoxide oxidation (Figs. 3 and 4). Hysteresis of the ignition and extinction temperature can also be attributed to different states of the surface of the catalyst at high and low activity.

The jump in conversion indicates that there is a change in the mechanism of the reaction. This is also shown by varying activation energy below and above ignition of 176 and 59 kJ/mol respectively [12]. At low activity, the conversion of carbon monoxide increases exponentially with temperature. The reaction proceeds via the Langmuir–Hinshelwood mechanism [42,46] where both carbon monoxide and oxygen adsorb on the surface of the catalyst to react to form carbon dioxide. The presence of carbon monoxide at the surface of platinum was reflected in the XANES spectra and EXAFS analysis and is generally observed by infra red spectroscopy [13,47,48]. Desorption of carbon monoxide is required to enable oxygen to adsorb and dissociate on the surface. The partial reaction order in carbon monoxide is close to −1 and for oxygen close

[2] See footnote 1.

to +1 for the carbon monoxide covered surface, which reflects the inhibiting effect of carbon monoxide on the rate of reaction [18,49]. With increasing temperature, there is enhanced production of carbon dioxide and decreasing concentration of carbon monoxide. The decrease in the coverage of carbon monoxide with temperature was reflected in the XANES spectra and is also well known in literature based on infra red spectroscopy [13,47,48].

The sudden switch in activity was paralleled by a change in the structure of the catalyst. The XANES spectra and EXAFS analysis showed a switch from the metallic to the partially oxidic state upon ignition and the reverse upon extinction. The low activity in the original state of the catalyst originates from the poisoning of the surface by carbon monoxide [12,47]. The high activity is a result of the exposure of surface sites of the catalyst after depletion of surface carbon monoxide. The low carbon monoxide concentration on the surface enabled oxygen to react to it forming an oxide layer. The result is a more active catalyst compared to the carbon monoxide poisoned catalyst. During ignition, the enhancement in conversion is paralleled by the formation of the oxide [16], a process, which proceeds auto-catalytically. The structural transformation of the nanoparticles we observe is, however, different from the surface reconstruction of the Pt(100) surface from a carbon monoxide-covered 1×1 phase to a hex phase saturated with adsorbed oxygen [8,9], which occurs under UHV conditions. Both these surfaces are still metallic. Our EXAFS analysis showed breaking of platinum–platinum bonds. SXRD measurements performed during carbon monoxide oxidation on a Pt(110) crystal [11] reported that the surface became covered with a distorted α-PtO_2; a commensurate and an incommensurate type, with the two types of oxides having a significantly higher reaction rate than the metallic surface. Recently, a monolayer of surface oxygen on rhodium, palladium, and platinum showed a hyperactivity, about two to three orders of magnitude greater than the surfaces that were poisoned by carbon monoxide [50]. However, our data do not suggest the presence of the α-PtO_2 phase or a chemisorbed layer of oxygen on our nanoparticles (vide infra).

In general, no or very little carbon monoxide adsorbed on a platinum catalyst in the high activity state is observed using infra red spectroscopy [13], which correlates to the partially oxidic state of platinum. The reactivity towards carbon monoxide may be so high that the concentration of carbon monoxide on either reduced or oxidized surface is too low to be detected. In contrast to the low activity regime, the reaction order is half in carbon monoxide and oxygen and the activation energy decreased to 59 kJ/mol [12]. This has also been attributed to a diffusion-limited surface reaction between adsorbed carbon monoxide and oxygen [43]. The change in the reaction order and activation energy indicates that the rate is not anymore limited by carbon monoxide desorption and subsequent oxygen activation. A high reactivity of a ruthenium surface oxide has often been described, and Mars van Krevelen [51] and Langmuir–Hinshelwood mechanisms [52] have been proposed.

4.2. Structure of the active oxide

Both XANES and EXAFS showed that the extent of oxidation, upon ignition, strongly depended on particle size [23,53] and support [24,25] as shown in Figs. 6 and 7. The higher the temperature of ignition was, the higher the extent of oxidation of the platinum particles. Thus Pt/TiO_2 was the least and Pt/SiO_2 the most oxidized. Pt/Al_2O_3 showed the opposite trend. With increasing temperature the solubility of oxygen in the metal increases [54]. With oxidation likely on the surface, our EXAFS analysis consistently showed that there was still a metal core left in all the oxidized catalysts. A larger metallic platinum core was left in the bigger particles. Based on the coordination numbers correlated to particle size [35], the extent of oxidation on s-Pt/Al_2O_3 was sufficient to completely cover its surface with an oxide layer, but it was just enough for b-Pt/Al_2O_3, which could therefore have metal sites exposed. The particles of s-Pt/Al_2O_3 deeply oxidized as did those of Pt/SiO_2. The amount of oxide on Pt/TiO_2 is insufficient to cover its surface completely. When increasing the amount of carbon monoxide at 207 °C over s-Pt/Al_2O_3, resulting in about 97% conversion, the XANES and EXAFS showed that there was a slight decrease in amount of oxide, but that the system did not switch to the low-activity regime. This shows that the structure of the catalyst is very dynamic and depends on the exact gas composition.

Using core level spectroscopy and density functional theory calculations [55], it was proposed that platinum ridges undergo 1-dimensional oxidation. The 1-D oxide stripes were found to be highly reactive in carbon monoxide oxidation due to the favorable transition states at the phase boundary. Because platinum nanoparticles have more edges, they are likewise expected to undergo 1-D oxidation as precursor to platinum oxidation. When a monolayer of oxygen adsorbs on the catalyst, it cannot desorb from the surface and platinum begins to oxidize [44]. Theory suggested that the surface of Pt(111) cannot be fully covered by oxygen [40,56], and that the highest coverage attainable with an O_2 oxidant is 0.5 monolayer [57]. The extent of oxidation strongly depends on the oxygen partial pressure [10]. The dependence of the heat of oxide formation to particle size has been studied [53] by calorimetric measurements. The evolved heat of oxide formation increased with decreasing particles size and the stoichiometry of the oxide approached that of PtO_2. These studies indicate that smaller particles tend to show more oxidation than single crystals. From SXRD [11] the surface oxide structure over Pt(110) during reaction conditions was found to be a thin distorted α-PtO_2, exhibiting a compressive and tensile strain relative to the bulk α-PtO_2 lattice. Bulk PtO_2 however displays low catalytic activity. The most oxidized spectrum at high activity (Pt/SiO_2) we obtained, had hints of post-edge features of β-PtO_2 [58] but with a whiteline intensity intermediate between the α-PtO_2 and β-PtO_2. These post-edge features were absent for the less oxidized spectra of Pt/Al_2O_3 and Pt/TiO_2. These observations suggest that the platinum oxide lacks long-range order, is distorted, and has a different structure than either α- or β-PtO_2. The Pt–Pt parameters obtained from fitting the oxidized s-Pt/Al_2O_3 spectrum appeared to be resulting from more than one Pt–Pt contribution. It could have come from the Pt–Pt contributions of the remaining metal core and of the oxide. The short Pt–O distance and low Pt–O coordination suggest a coordination that is lower than octahedral, such as the square-planar configuration in PtO and Pt_3O_4 [59]. Calculations have predicted that Pt_3O_4 is active for oxidation, as carbon monoxide binds strongly to the undercoordinated oxygen at the surface and that PtO_2 can be active, when it contains many surface defects [41]. Likewise, in-situ XRD showed that oxygen covered particles during carbon monoxide oxidation were composed of combined metallic, PtO, and Pt_3O_4 clusters [15]. However, the platinum oxide that we observed is characterized by disorder and a significant fraction of defects. Our oxide structure does not resemble a surface that is partially covered with oxygen that showed hyperactivity [50], nor does it resemble bulk PtO_2 that showed low activity [60]. Under-coordination at the surface of the nanoparticles, strain, and partial oxidation are the key phenomena responsible for the high catalytic activity.

5. Conclusion

Carbon monoxide oxidation on supported platinum catalysts exhibits two activity regimes: low activity at high carbon monoxide concentration and low temperature and high activity at low carbon monoxide concentration and high temperature. There is ignition when going from low to high activity and there is extinction when going from high to low activity. The catalyst at low activity

is metallic covered with carbon monoxide, which hampers oxygen from reacting. At high activity, the particles are partially oxidic. Our data suggest that a disordered surface oxide has formed that is rich in defects and with a platinum coordination that is possibly square planar. The depletion of carbon monoxide at high activity enables oxygen to interact with the surface, and enhances the catalytic activity by changing the rate-limiting step. The thickness of the disordered oxide layer strongly depends on particle size and the support and could be partially related to the temperature at which it formed. Among the supported catalysts, Pt/TiO_2 reached high activity at the lowest temperature and Pt/SiO_2 needed the highest temperature to reach high activity. Pt/Al_2O_3 showed an intermediate temperature.

Acknowledgments

E.M.C.A. thanks the European Commission for an Erasmus Mundus (MaMaSELF) grant. J.A.v.B. and J.S. acknowledge the Swiss National Science Foundation for the granted research fund. We thank Dr. Frank Krumreich, of the ETH Zurich, for measuring the TEM micrographs.

References

[1] B.M. Weckhuysen, Phys. Chem. Chem. Phys. 5 (2003) 4351.
[2] J.A. van Bokhoven, T. Ressler, F.M.F. de Groot, G. Knopp-Gericke, in: B.M. Weckhuysen (Ed.), In-Situ Spectroscopy of Catalysts, American Scientific Publishers, California, 2004, p. 123.
[3] D.C. Koningsberger, B.L. Mojet, G.E. van Dorssen, D.E. Ramaker, Top. Catal. 10 (2000) 143.
[4] D.E. Ramaker, D.C. Koningsberger, Phys. Rev. Lett. 89 (2002) 139701.
[5] A.L. Ankudinov, J.J. Rehr, J.J. Low, S.R. Bare, Phys. Rev. Lett. 89 (2002) 139702.
[6] O.V. Safonova, M. Tromp, J.A. van Bokhoven, F.M.F. de Groot, J. Evans, P. Glatzel, J. Phys. Chem. B 110 (2006) 16162.
[7] J.M. Zalc, D.G. Löffler, J. Power Sources 111 (2002) 58.
[8] G. Ertl, P.R. Norton, J. Rüstig, Phys. Rev. Lett. 49 (1982) 177.
[9] R. Imbihl, M.P. Cox, G. Ertl, J. Chem. Phys. 84 (1986) 3519.
[10] B.L.M. Hendriksen, J.W.M. Frenken, Phys. Rev. Lett. 89 (2002) 046101.
[11] M.D. Ackermann, T.M. Pedersen, B.L.M. Hendriksen, O. Robach, S.C. Bobaru, I. Popa, C. Quiros, H. Kim, B. Hammer, S. Ferrer, J.W.M. Frenken, Phys. Rev. Lett. 95 (2005) 255505.
[12] G.A. Somorjai, Appl. Surf. Sci. 121/122 (1997) 1.
[13] F.J. Gracia, L. Bollmann, E.E. Wolf, J.T. Miller, A.J. Kropf, J. Catal. 220 (2003) 382.
[14] B.C. Sales, J.E. Turner, M.B. Maple, Surf. Sci. 114 (1982) 381.
[15] N. Hartmann, R. Imbihl, W. Vogel, Catal. Lett. 28 (1994) 373.
[16] J. Singh, E.M. Alayon, M. Tromp, O. Safonova, P. Glatzel, M. Nachtegaal, R. Frahm, J.A. van Bokhoven, Angew. Chem. Int. Ed. 47 (2008) 9260.
[17] B. Atalik, D. Uner, J. Catal. 241 (2006) 268.
[18] J. Yang, V. Tschamber, D. Habermacher, F. Garin, P. Gilot, Appl. Catal. B 83 (2008) 229.
[19] D.E. Ramaker, G.E. van Dorssen, B.L. Mojet, D.C. Koningsberger, Top. Catal. 10 (2000) 157.
[20] M. Vaarkamp, J.T. Miller, F.S. Modica, D.C. Koningsberger, J. Catal. 163 (1996) 294.
[21] T. Visser, T.A. Nijhuis, A.M.J. van der Eerden, K. Jenken, Y. Ji, W. Bras, S. Nikitenko, Y. Ikeda, M. Lepage, B.M. Weckhuysen, J. Phys. Chem. B 109 (2005) 3822.
[22] A. Saramat, P. Thormählen, M. Skoglundh, G.S. Attard, A.E.C. Palmqvist, J. Catal. 253 (2008) 253.
[23] Y. Yazawa, H. Yoshida, T. Hattori, Appl. Catal. A 237 (2002) 139.
[24] M. Kobayashi, A. Morita, M. Ikeda, Appl. Catal. B 71 (2007) 94.
[25] A.Y. Stakheev, L.M. Kustov, Appl. Catal. A 188 (1999) 3.
[26] N. Weiher, E. Bus, B. Gorzolnik, B. Möller, R. Prins, J.A. van Bokhoven, J. Synch. Rad. 12 (2005) 675.
[27] F.W.H. Kampers, T.M. Maas, J. van Grondelle, P. Brinkgreve, D.C. Koningsberger, Rev. Sci. Instrum. 60 (1989) 2635.
[28] M. Vaarkamp, J.C. Linders, D.C. Koningsberger, Physica B 208/209 (1995) 159.
[29] E. Bus, J.A. van Bokhoven, J. Phys. Chem. C 111 (2007) 9761.
[30] B. Ravel, J. Synch. Radiat. 8 (2001) 314.
[31] A.L. Ankudinov, B. Ravel, J.J. Rehr, S.D. Conradson, Phys. Rev. B 58 (1998) 7565.
[32] M. Rinnemo, D. Kulginov, S. Johansson, V.P. Zhdanov, B. Kasemo, Surf. Sci. 376 (1997) 297.
[33] S. Salomons, R.E. Hayes, M. Votsmeier, A. Drochner, H. Vogel, S. Malmberg, J. Gieshoff, Appl. Catal. B 70 (2007) 305.
[34] A.Y. Rozovskii, M.A. Kipnis, E.A. Volnina, G.I. Lin, P.V. Samokhin, Kinet. Catal. 48 (2007) 701.
[35] A.I. Frenkel, C.W. Hills, R.G. Nuzzo, J. Phys. Chem. B 105 (2001) 12689.
[36] M.K. Oudenhuijzen, J.H. Bitter, D.C. Koningsberger, J. Phys. Chem. B 105 (2001) 4616.
[37] E. Bus, J.T. Miller, A.J. Kropf, R. Prins, J.A. van Bokhoven, Phys. Chem. Chem. Phys. 8 (2006) 3248.
[38] J.T. Miller, A.J. Kropf, Y. Zha, J.R. Regalbuto, L. Delannoy, C. Louis, E. Bus, J.A. van Bokhoven, J. Catal. 240 (2006) 222.
[39] L.L. Wang, D.D. Johnson, J. Am. Chem. Soc. 129 (2007) 3658.
[40] N. Seriani, W. Pompe, L.C. Ciacchi, J. Phys. Chem. B 110 (2006) 14860.
[41] A. Urakawa, T. Burgi, H.P. Schläpfer, A. Baiker, J. Chem. Phys. 124 (2006) 054717.
[42] T.H. Lindstrom, T.T. Tsotsis, Surf. Sci. 150 (1985) 487.
[43] X. Su, P.S. Cremer, Y.R. Shen, G.A. Somorjai, J. Am. Chem. Soc. 119 (1997) 3994.
[44] F. van Neer, A. Bliek, Chem. Eng. Sci. 54 (1999) 4483.
[45] R. Burch, P.K. Loader, Appl. Catal. B 5 (1994) 149.
[46] T.A. Nijhuis, M. Makkee, A.D. van Langeveld, J.A. Moulijn, Appl. Catal. A 164 (1997) 237.
[47] P.T. Fanson, W.N. Delgass, J. Lauterbach, J. Catal. 204 (2001) 35.
[48] D.M. Haaland, F.L. Williams, J. Catal. 76 (1982) 450.
[49] R.H. Nibbelke, M.A.J. Campman, J.H.B.J. Hoebink, G.B. Marin, J. Catal. 171 (1997) 358.
[50] M.S. Chen, Y. Cai, Z. Yan, K.K. Gath, S. Axnanda, D. Wayne Goodman, Surf. Sci. 601 (2007) 5326.
[51] H. Over, Y.D. Kim, A.P. Seitsonen, S. Wendt, E. Lundgren, M. Schmid, P. Varga, A. Morgante, G. Ertl, Science 287 (2000) 1474.
[52] C. Stampfl, M. Scheffler, Phys. Rev. Lett. 78 (1997) 1500.
[53] C.B. Wang, H.K. Lin, S.N. Hsu, T.H. Huang, H.C. Chiu, J. Mol. Catal. A 188 (2002) 201.
[54] M. Salmeron, L. Brewer, G. Somorjai, Surf. Sci. 112 (1981) 207.
[55] J.G. Wang, W.X. Li, M. Borg, J. Gustafon, A. Mikkelsen, T.M. Pedersen, E. Lundgren, J. Weissenrieder, J. Klikovits, M. Schmid, B. Hammer, J.N. Andersen, Phys. Rev. Lett. 95 (2005) 256102.
[56] A.D. Smeltz, R.B. Getman, W.F. Schneider, F.H. Ribeiro, Catal. Today 136 (2008) 84.
[57] R.B. Getman, Y. Xu, W. Schneider, J. Phys. Chem. C 112 (2008) 9559.
[58] A.N. Mansour, D.E. Sayers, J.W. Cook Jr., D.R. Short, R.D. Shannon, J.R. Katzer, J. Phys. Chem. 88 (1984) 1778.
[59] N. Seriani, J. Zin, W. Pompe, L.C. Ciacchi, Phys. Rev. B 76 (2007) 155421.
[60] L. Olsson, E. Fridell, J. Catal. 210 (2002) 340.